Regular Article

PHYSICAL CHEMISTRY RESEARCH
Published by the
Iranian Chemical Society
www.physchemres.org
info@physchemres.org

Phys. Chem. Res., Vol. 8, No. 2, 281-295, June 2020
DOI: 10.22036/pcr.2020.210668.1704

A Novel Poly(vinyl alcohol) Post-precipitation Template Synthesis and Property Tuning of Photoactive Mesoporous Nano-TiO_2

A. Hamisu[a,b], U.I. Gaya[b,*] and A.H. Abdullah[c,d]

[a]*Department of Chemistry, Kano University of Science and Technology Wudil, P.M.B. 3244 Kano, Nigeria*
[b]*Department of Pure and Industrial Chemistry, Bayero University Kano, 700241 Kano, P.M.B. 3011, Kano State, Nigeria*
[c]*Department of Chemistry, Faculty of Science, Universiti Putra Malaysia, 43400 UPM Serdang, Selangor D.E., Malaysia*
[d]*Institute of Advanced Technology, Universiti Putra Malaysia, 43400 UPM Serdang, Selangor D.E., Malaysia*

(Received 6 December 2019, Accepted 24 February 2020)

For the first time, a facile method is introduced to obtain ultrathin, mesoporous TiO_2 nanosheets by the alkali precipitation of aqueous $TiCl_3$ in the presence of NH_4OH, and in-situ templating with polyvinyl alcohol (PVA). The synthesized titania nanosheets have been characterized by N_2 adsorption-desorption measurements, x-ray diffraction (XRD), scanning electron microscopy (SEM), transmission electron microscopy (TEM), thermo-gravimetric analysis (TGA) and ultraviolet-visible (UV-Vis) spectroscopy. The titania obtained were hexagonal-like, detached, non-agglomerated, polydispersed, sub-20 nm nanodiscs. Their absorption gap edges, surface area and pore volumes can easily be tailored by simply tuning the amount of the template. Accordingly, their aggregation as microspheres can successfully be controlled by the templating step. The remarkable photoactivity of these nanoscopic materials has been confirmed by the degradation of aqueous methyl orange.

Keywords: Anatase, Mesoporous, TiO_2, Template, Photocatalysis, Precipitation

INTRODUCTION

Much attention has been paid to the building of nanostructured materials for possible utilization in a variety of applications including photocatalysis, solar cells, lithium rechargeable batteries, sensors and hydrogen evolution [1,2]. Mesoporous TiO_2 has particularly become extraordinarily attractive due to its controllable properties, large surface area, desirable adsorption capacity, good permeability, and high photocatalytic activity under UV light irradiation [3-6]. It was firstly synthesized *via* sol-gel route and surfactant templating [7]. Additionally, panoptic efforts have awakened interest in the synthesis of TiO_2 mesostructures by other chemical methods such as the hydrothermal, evaporation-induced self-assembly, and precipitation [8-10]. In all methods, an array of TiO_2 precursors are described which include titanium alkoxides [11], $TiOSO_4$ [12] and titanium chlorides [13]. Similarly, an array of templates such as a surfactant, homopolymer, block copolymer, small non-surfactant organic molecule, microemulsion droplet, have been used in the preparation of TiO_2 mesostructure [14-17]. However, how to obtain mesoporous TiO_2 with stable and controllable mesostructures, including high surface area and pore volumes/sizes, remains a major challenge for the researchers working in this field. By far, after calcination, mesoporous TiO_2 still shows low surface area and small pore size due to either the uncontrollable hydrolysis/condensation reaction with water (which is difficult to match with the self-assembly process with the templates), or the poor thermal stability of the mesostructure and subsequent collapse upon calcination [2].

Titanium dioxide is the most popular transition-metal oxide semiconductor for photocatalytic applications because

*Corresponding author. E-mail: uigaya.chm@buk.edu.ng

of its unique physical, chemical and optical properties such as high oxidizing power, high stability, low cost, non-toxicity, resistance against photocorrosion and chemical corrosion, and ability to mineralize refractory organic pollutants under ambient pressure and temperature [18-20]. Arguably, anatase is the most common and widely recognized photoactive TiO_2 phase followed by rutile and brookite. The anatase titania with small particle sizes and high crystallinity are usually desirable [21]. Currently, however, the synthesis of this material with high quality is a challenge. For example, Xiao *et al*. [22] prepared a nano-anatase, though they faced a significant mesopore collapse. Similarly, Mao-Xiang *et al.* [23] prepared some mesoporous anatase titania with high a surface area by a precipitation method; however, the particle sizes of these materials were large. In the latter case, measures such as templating could have possibly preserved the mesopores.

Polyvinyl alcohol (PVA), with a chemical formula $[CH_2CH(OH)]_n$, is a water-soluble [24], non-toxic, hydrophilic, biodegradable and biocompatible synthetic plastic polymer, suitable for various applications [25] due to its remarkable properties such as flexibility, adhesion, emulsifying and tensile strength [26] and a high Young's modulus [27]. There has been an increasing attention to the application of PVA in nano-materials production for flexibility modification [26]. Accordingly, it has been used as a template in preparation of porous materials [24,27-29]. In this work, a new post-precipitation template synthesis of mesoporous TiO_2, in which the template is applied after precipitating the TiO_2 precursor ($Ti(OH)_4$) is for the first time reported. The PVA and titanium (III) chloride ($TiCl_3$) solution is used as a template and source of titanium, respectively. The photocatalytic activities of the synthesized mesoporous TiO_2 were evaluated by measuring the photocatalytic degradation of methyl orange (MO) in water under UV light irradiation.

EXPERIMENTAL

Materials

The titanium(III) chloride ($TiCl_3$, 15% w/v) solution was purchased from BDH. Poly (vinyl alcohol) (PVA, $[-CH_2CH(OH-)]_n$, M_w = 130,000 g mol^{-1}, 99 + %hydrolyzed), was purchased from Sigma-Aldrich. The ammonium hydroxide (NH_4OH, 30%) solution, nitric acid (HNO_3, 65%), methyl orange (MO, 85%), sulfuric acid (H_2SO_4, 95-98%) and sodium hydroxide (NaOH) were purchased from R & M Chemicals. Preparation of aqueous solutions was made using deionized water.

Catalyst Preparation

Titanium(III) chloride (20 ml) was slowly added to 300 ml of deionized water and stirred for 20 min. Subsequently, the pH of this solution was adjusted by adding 18 ml of NH_4OH, with stirring for 4 h, until white precipitates were formed. The precipitates were washed several times with deionized water until neutrality, and then acidified with 200 ml of dilute nitric acid (0.5 M). The resulting suspension was stirred for 1 h. In order to prepare the templated titania ($0.25PV/TiO_2$, $0.5PV/TiO_2$ and $1PV/TiO_2$), 0.25 g, 0.5 g, and 1.0 g of PVA solution (30 ml) were added slowly with continuous stirring, at 75 °C for 4 h. The mixture was kept overnight at room temperature, then it was dried on a heating mantle at 110 °C, and finally calcined in air at 450 °C for 4 h. Template-free TiO_2 ($0PV/TiO_2$) was prepared in a similar manner, without PVA addition.

Characterization

In order to determine specific surface area and pore volume, nitrogen adsorption-desorption measurements were performed based on Brunauer-Emmett-Teller (BET) method using Micromeritics 3Flex 1.02 instrument at 77.322 K. Sample mass was 0.1279 g. Atmospheric gases, organics and other adsorbed species possibly present on the samples were outgassed at 200 °C for 2 h. The crystalline phase of the catalysts was characterized by powder X-ray diffraction (PXRD) using a Shimadzu XRD-6000 X-Ray diffractometer, and sizes were estimated using Scherer and Williamson-Hall methods. This facility was operated with a Cu Kα radiation (λ = 0.15406 nm) and in the 2θ range of 20-80°. Rietveld profile refinement of the structures was carried out using FullProf suite version 6.30. The morphology, structure and thickness of the catalyst particles were examined using field emission scanning electron microscope (FE-SEM) from NOVA NANOSEM 230 and a JEM-2100F transmission electron microscope. The energy dispersive X-ray (EDX) spectra of catalyst elements were

recorded on a NOVA NANOSEM 230 FE-SEM. The band gap of the catalysts was determined based on absorption data recorded on a Shimadzu UV-3600 UV-VIS-NIR spectrophotometer. Barium sulfate was used as a reference material and scan range was limited to 220-800 nm. The decomposition of PVA in the precursor was monitored by thermo-gravimetric analysis (TGA) using a METTLER TOLEDO TGA/DSC 1 STAR^e System, heated at 10 °C min^{-1} under N_2 atmosphere.

Photoexperiments

The photocatalytic activity of the synthesized catalysts was evaluated in relative terms by monitoring the percentage of methyl orange degraded. Experiments were carried out in a previously described photoreactor [30]. The reactor was fitted with a new 3 W China model E14 GMY UV lamp (UV intensity = 450 μw cm^{-2}, wavelength = 253 nm). The catalysts having the highest BET surface area, BET pore volume, and catalytic performance (0.5PV/TiO_2) were selected for use in the degradation studies. Optimum values of the three independent variables (TiO_2 loading, initial concentration of MO and pH) for the degradation of MO (pH = 2.5, nano-TiO_2 = 1 g l^{-1} and initial MO concentration of 25 mg l^{-1}) were utilized in the photocatalytic experiments.

In a typical photocatalytic experiment, a solution containing the desired amount of MO and catalyst was added to the photoreactor. Solution pH was adjusted using NaOH and H_2SO_4. During the reaction process, oxygen was continuously bubbled through the mixture to avoid changing the concentration of dissolved oxygen. Test samples were taken at periodic intervals of time and filtered using cellulose nitrate membrane (0.45 μm). The residual concentration of MO solution was measured at 465.4 nm using Perkin Elmer Lambda 35 UV-Vis spectrometer. The percent degradation of the initial methyl orange concentration was calculated using Eq. (1),

$$\%Degradation = \frac{[MO]_0 - [MO]_t}{[MO]_0} \quad (1)$$

where $[MO]_o$ is the initial methyl orange concentration, and $[MO]_t$ is the concentration of methyl orange at irradiation time *t*. In order to determine the kinetic parameters, experiments were performed at optimum conditions for 120 min. Kinetic profiles were plotted according to pseudo-zero-order. These plots were compared using the coefficient of determination (R^2) of their curves.

RESULT AND DISCUSSION

Catalyst Surface Area and Crystalline Properties

The N_2 adsorption-desorption isotherms for 0.25PV/TiO_2, 0.5PV/TiO_2, and 1PV/TiO_2 are displayed by Fig. 1A, B and C, respectively. Based on IUPAC classification, these PVA containing samples can exhibit type IV isotherms [31]. For all of the titania, mesoporosity is readily confirmed by the presence of hysteresis loops and obvious condensation/evaporation steps within partial pressure range of 0.6-0.9.

The surface area and pore volume were estimated using Brunauer-Emmett-Teller (BET) and Barrett-Joyner-Halenda (BJH) methods. Figure 2 depicts the BET surface area plot (top set) and BJH adsorption cumulative pore volume (bottom set). The surface area, pore volumes and sizes of these catalysts are shown in Table 1. It can be observed that the values of BET surface area and pore volume increase proportionally with an increase in PVA. Therefore, the BET surface area of 0.25PV/TiO_2 increases from 73.25 m^2 g^{-1} to 97.4042 m^2 g^{-1} in 0.5 PV/TiO_2. However, on further increase in PVA to 1 g, a decrease in these properties is generally observed perhaps due to an exceedingly high amount of the template. Similar observations were made by Liu *et al*. [32] and Nguyen *et al*. [2] upon application of P123 and ethylene glycol as templates in the synthesis of mesoporous TiO_2, respectively. In this study, the highest BET surface area and pore volume were obtained with 0.5PV/TiO_2, implying that only an optimum PVA template can play a positive role in the post-precipitation templating.

In order to study the crystalline structures of the synthesized TiO_2 photocatalyst, X-ray diffractograms were collected (Fig. 3). Rietveld profile refinement of the structures was carried out using FullProf suite version 6.30. As seen from the figure, all the catalyst specimens show anatase peaks at 2θ (and planes) at 25.44° (101), 38.07° (004), 48.12° (200), 54.02° (105), 55.21° (211), 62.76° (204), 70.01° (116), and 94.92° (215). Interestingly, neither brookite nor rutile phases is shown, even after the

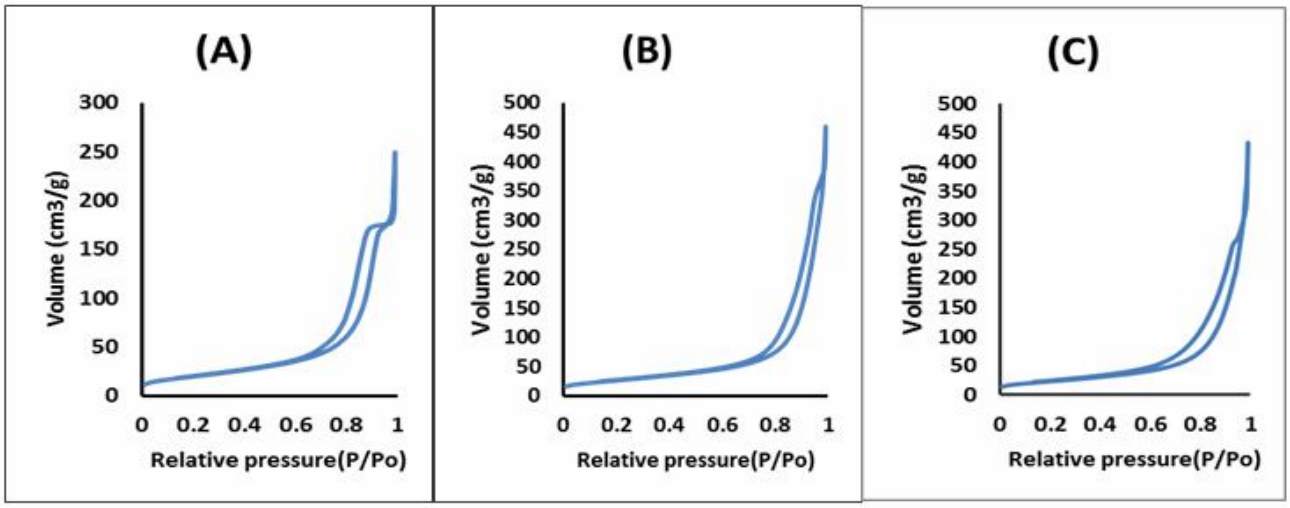

Fig. 1. The N_2 adsorption-desorption isotherm for 0.25PV/TiO_2 (A), 0.5PV/TiO_2 (B) and 1PV/TiO_2 (C).

Table 1. The Surface Properties of Titania Obtained from N_2 Adsorption-desorption Data

Sample	Scherer crystal size (nm)	Surface area ($m^2\ g^{-1}$)	Pore volume ($cm^3\ g^{-1}$)	Pore size (Å)	
				Adsorption	Desorption
0.25PV/TiO_2	10.22	73.2513	0.385254	203.9197	210.3735
0.5PV/TiO_2	8.68	97.4042	0.713045	281.2305	292.8189
1PV/TiO_2	9.23	82.7001	0.670765	315.8560	324.4327

modification of TiO_2 by templating. The lattice parameters for the refined anatase structure are a = 3.81 Å, b = 3.81 Å and c = 8.64 Å.

The crystallite sizes of the obtained catalysts 0PV/TiO_2, 0.25PV/TiO_2, 0.5PV/TiO_2 and 1PV/TiO_2 as calculated using the Scherer equation were 12.07, 10.22, 8.68 and 9.23 nm, respectively. Table 1 shows its inverse relationship between the sizes of the particles and their surface area. The estimated sizes show no broadening or strain, having offered a correlation coefficient of 0.9439 when compared with those derived from Williamson-Hall data. Unlike in this study, TiO_2 of similar particle sizes prepared by a majority of workers previously, either were mostly biphasic and hierachichal macro-/mesoporous [33] or underwent a redshift due to the modification effects [34].

Catalyst Morphology and Composition

In order to depict the structure and form of the obtained titania, field emission scanning electron microscopy (FE-SEM) measurements were performed. The results are displayed in Fig. 4. It can be seen from the Fig. 4a that the template-free 0PV/TiO_2 shows aggregates of titania crystals. Figure 4b however shows a mesostructured 0.25PV/TiO_2, but with a lesser aggregation of the titania crystals. In contrast with the aforementioned, deaggregated mesostructures were observed with the 0.5PV/TiO_2

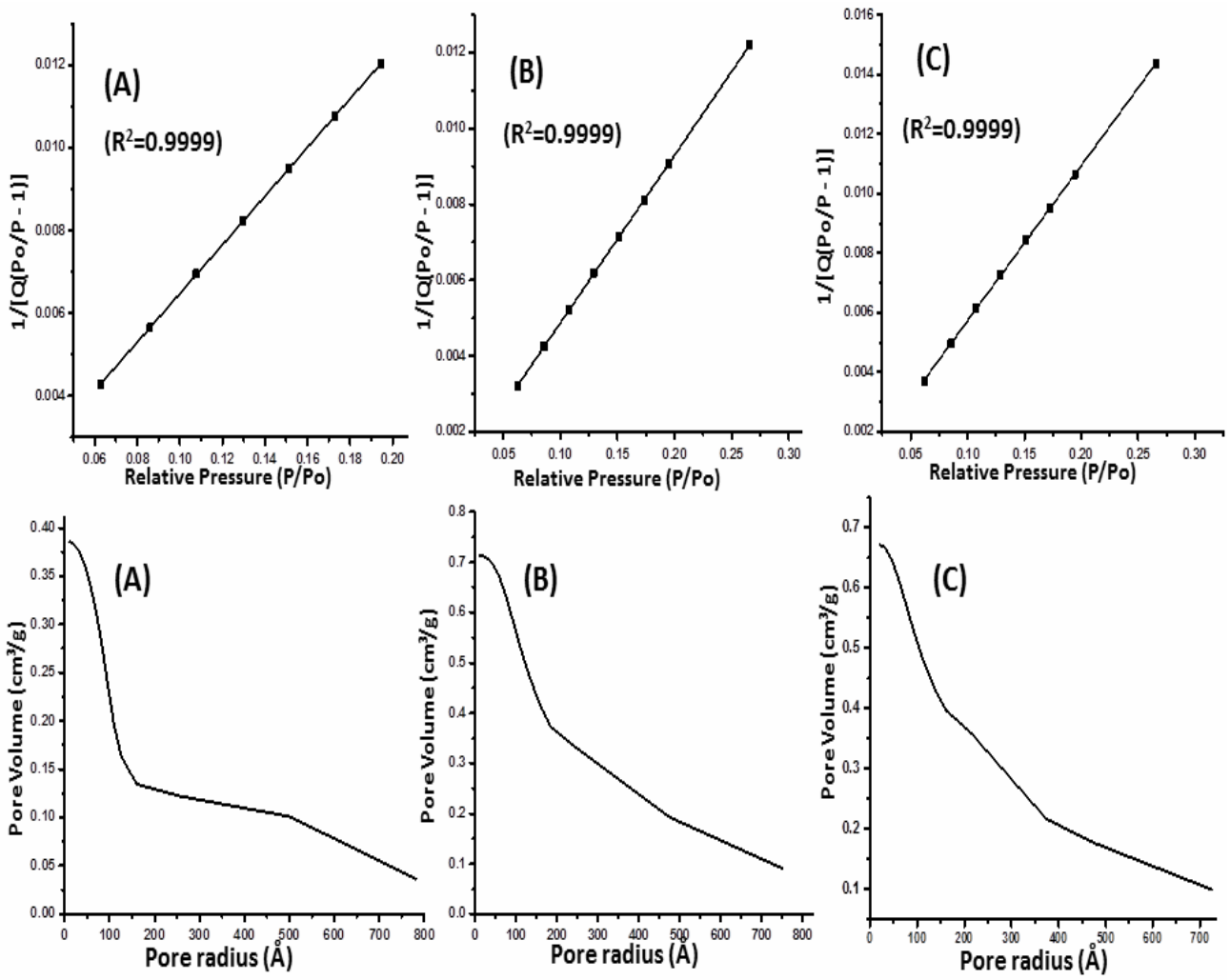

Fig. 2. The BET surface area plot (top) and BJH adsorption cumulative pore volume (bottom) for (A) 25PV/TiO_2, (B) 0.5PV/TiO_2 and (C) 1PV/TiO_2.

(Fig. 4c). This observation correlates with the BET surface areas in Table 1, indicating a higher surface area with an increase in the amount of PVA template.

The TEM images and size distribution curve of 0.25PV/TiO_2 are shown in Fig. 5. The hexagonal-like shaped 2D catalyst particles are readily visualized from Fig. 5A and Fig. 5B at different magnifications. The average particle sizes of the photocatalysts were determined from the images using ImageJ software (Java 1.6.0). The 0.25PV/TiO_2 (Fig. 5) has an average size of 12.69 nm (Fig. 5C). Similarly, the major catalyst (0.5PV/TiO_2) shows a similar shape (Fig. 6) with an average particle size of 9.49 nm. The estimated particle sizes correlate fairly well with those obtained by using Scherer equation. The average size of the optimal catalyst (0.5PV/TiO_2) declined from that of 0.25PV/TiO_2 due to improved surface area and minimal deaggregation. The interplanar space of the nanodiscs is 0.323 nm (Fig. 6), which corresponds to the (101) crystal facets of anatase TiO_2 [35].

The chemical composition of the photocatalyst was confirmed using energy dispersive x-ray (EDX) analysis. Figure 7 shows the EDX spectra of 0.5PV/TiO_2. As seen

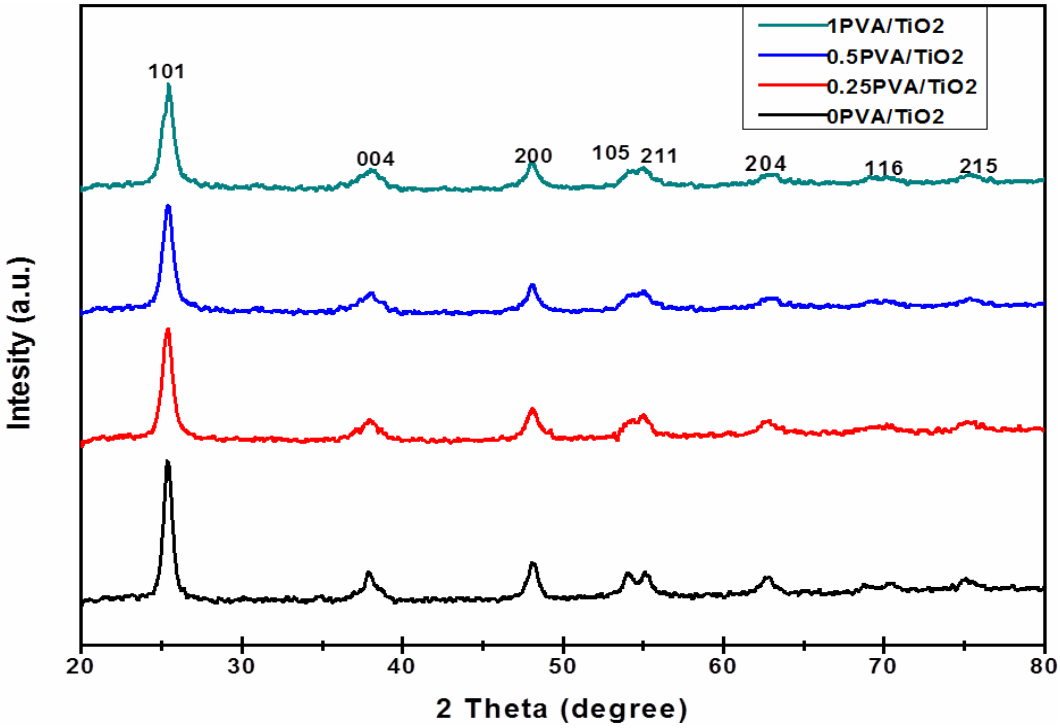

Fig. 3. The XRD patterns of the prepared titania with and without PVA.

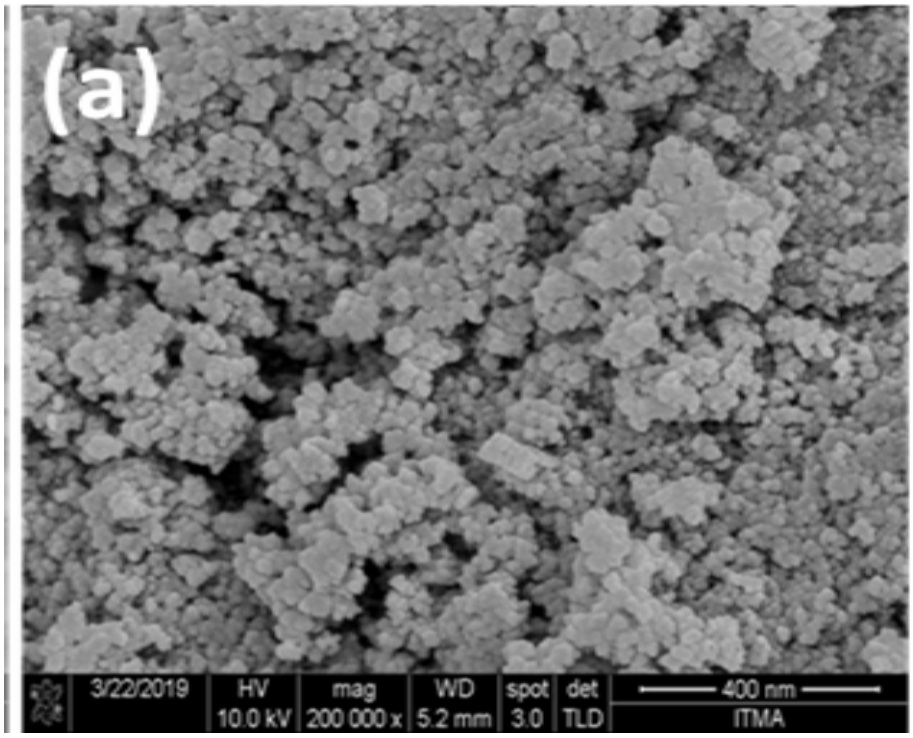

Fig. 4. The FE-SEM images of the synthesized titania (a) 0PV/TiO_2 (b), 0.25/TiO_2 and (c) 0.5PV/TiO_2.

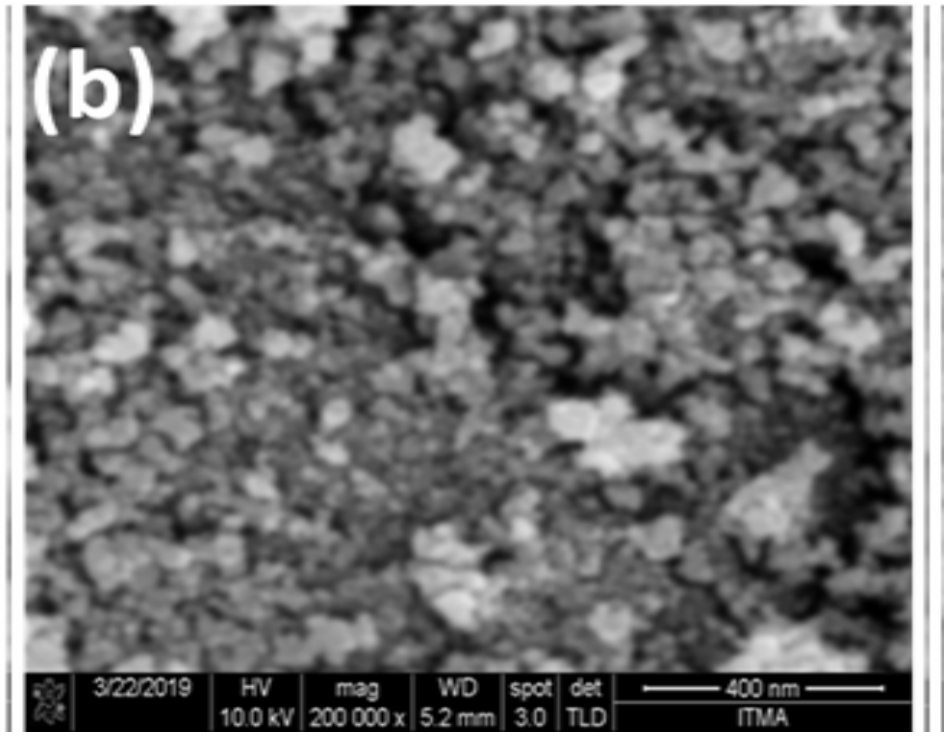

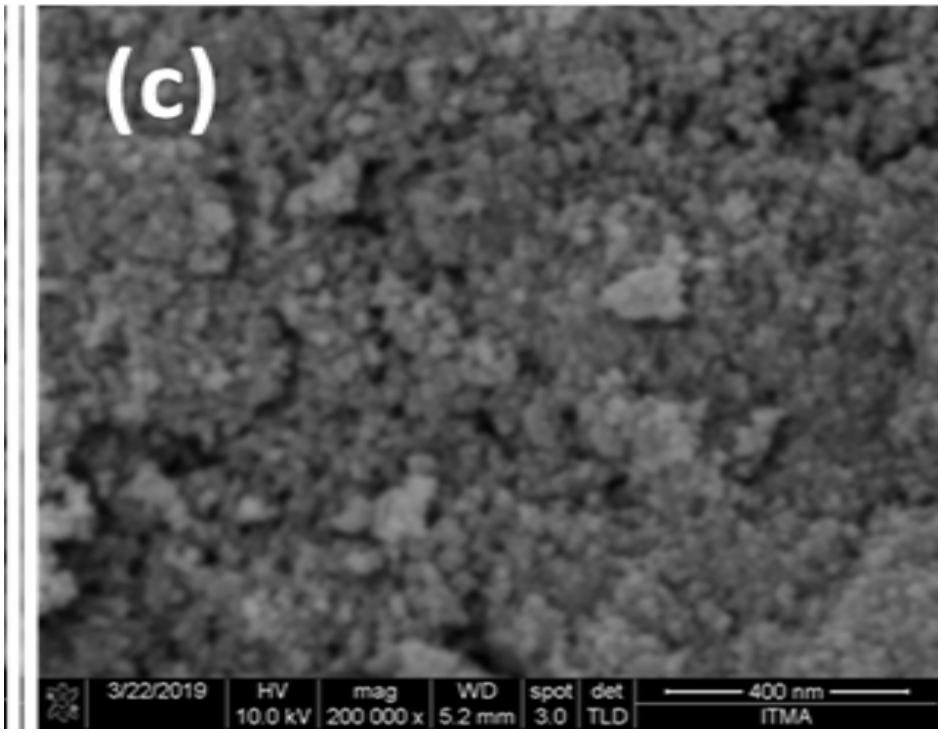

Fig. 4. Continued.

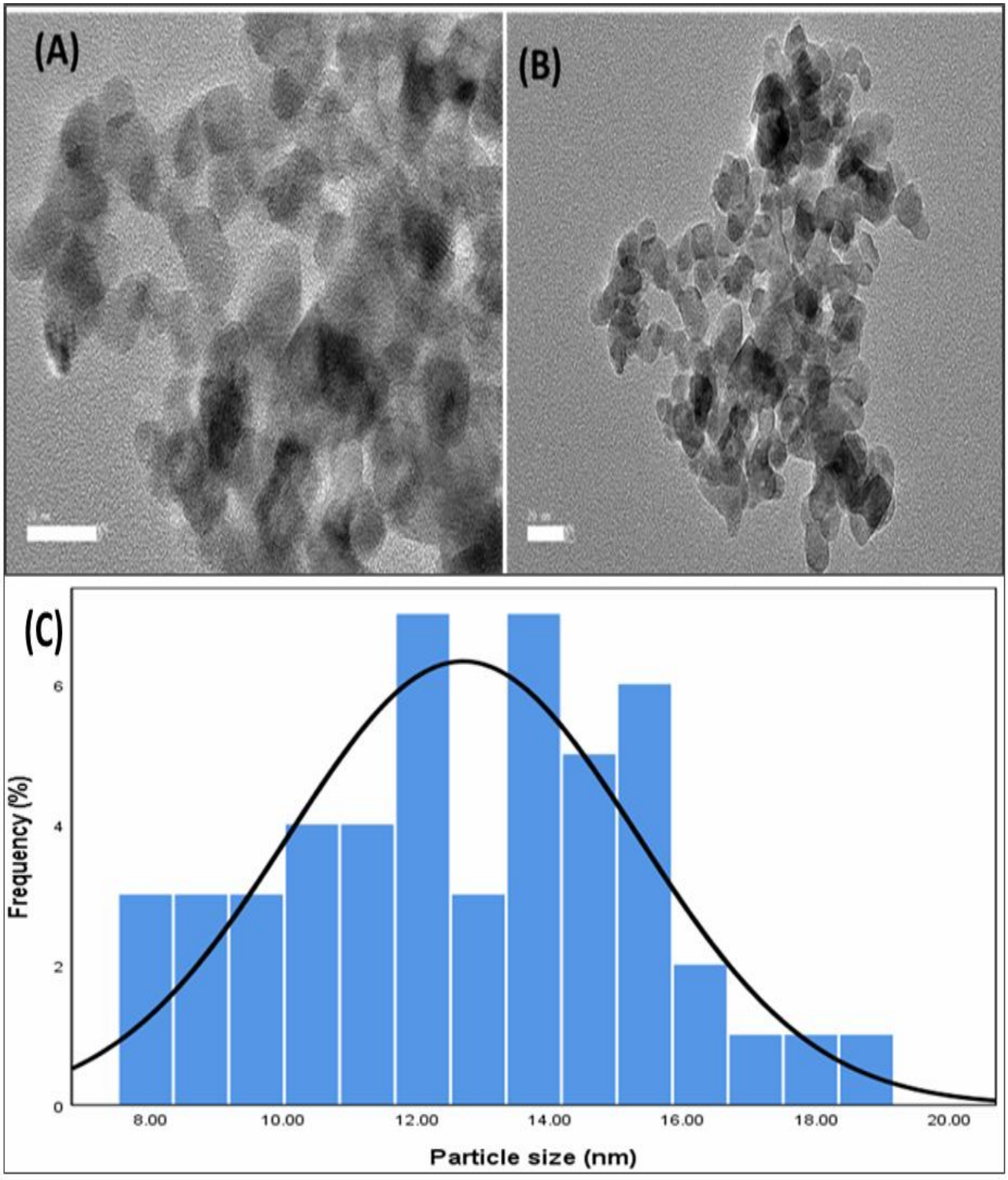

Fig. 5. (A, B) The TEM images of 0.25PV/TiO_2 at different magnifications, and (C) the size distribution curve of 0.25PV/TiO_2. Scale: 20 nm.

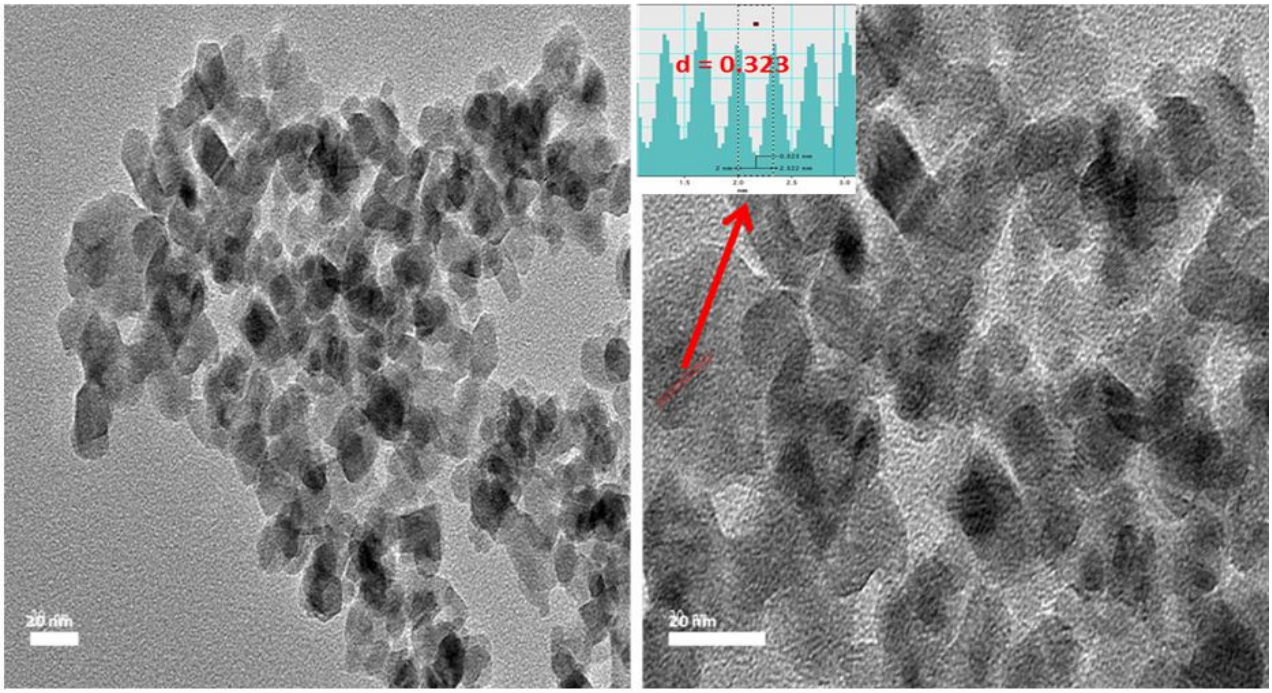

Fig. 6. The TEM image of 0.5PV/TiO_2 at different magnifications. Scale: 20 nm.

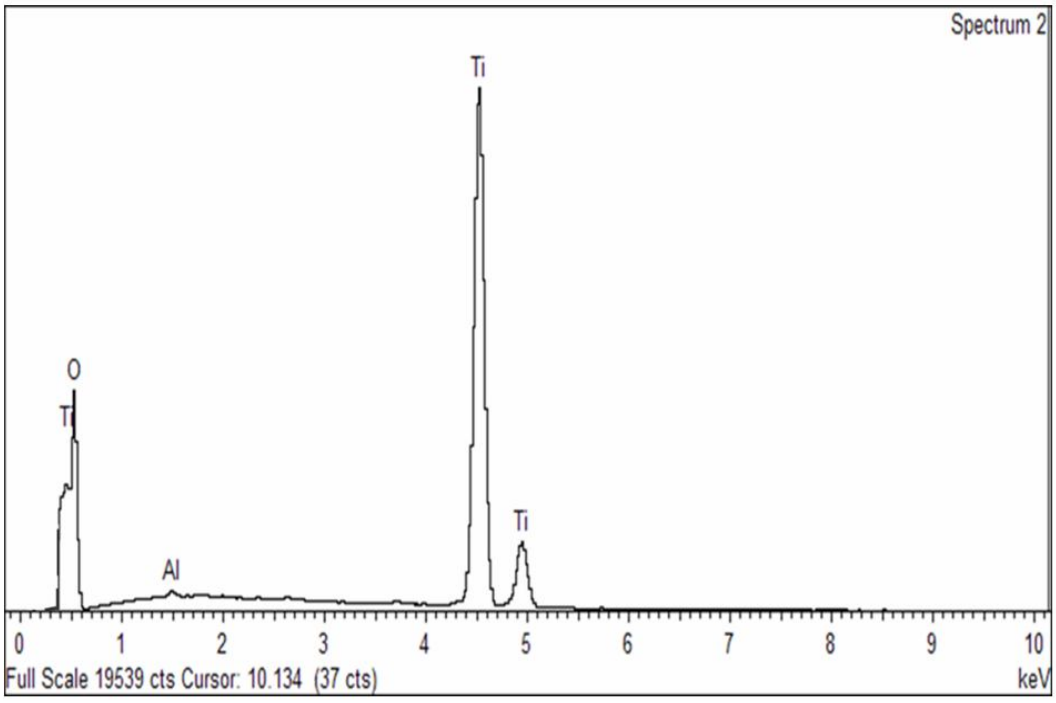

Fig. 7. The EDX spectra of 0.5PV/TiO_2.

in the figure, the major peaks are for Ti and O, which confirms the prepared catalyst to be TiO_2. From the distribution, the Ti to O atomic ratio is 1: 0.4652, indicating the stoichiometry in TiO_2.

Thermogravimetric Analysis

Thermogravimetric analysis (TGA) was performed to determine the content of PVA template in the catalysts and stability of the prepared photocatalysts during the post-synthesis stage. Naturally, plastic polymers undergo several changes when subjected to a high temperature with the release of gases and or liquids of different shapes, colors and molecular weights [36]. In the first stage of the synthesis of 0.5PV/TiO_2, $Ti(OH)_4$ is precipitated. The TGA curve of PVA/$Ti(OH)_4$ hybrid corresponding to the 0.5PV/TiO_2 precursor at a heating rate of 10 °C min^{-1} is shown in Fig. 8.

The thermogram of the 0.5PV/TiO_2 precursor (Fig. 8) consists of three steps. The first step is a weight loss near 100 °C, corresponding to the volatile and physically adsorbed water. This step is followed by a stepwise PVA decomposition - a partial PVA weight loss (*ca.* 16%) in the temperature range of 150-370 °C followed by another partial weight loss (*ca.* 5%) in the temperature range of 370-455 °C. The latter stages are due to the decomposition of PVA main chain into smaller parts and complete pyrolysis, respectively [36]. No weight loss was observed above 455 °C, indicating that pyrolysis has been fully achieved, leaving behind only the stable and crystallized TiO_2. Generally and in agreement with this study, PVA has been reported to decompose completely around 450 °C [36-38].

Band Gap Analysis

The optical absorptions of the synthesized photocatalysts were studied using UV-Vis analysis and computed based on the band gap energy-wavelength equation (Eq. (2)) [39]. The shifts in these energies are displayed in Fig. 9.

$$E_g = \frac{hc}{\lambda} \tag{2}$$

where E_g is the band-gap energy (eV), h is Planck's constant, and c is the velocity of light. Moreover, λ is the wavelength (nm) corresponding to the intersection point of the wavelength axis and the tangent to the absorbance curve. From Fig. 9, the band-gap energies of 0PV/TIO_2, 0.25PV/TiO_2, 0.5PV/TiO_2 and 1PV/TiO_2 were 3.04, 2.95, 2.69 and 2.87 eV, respectively. These results illustrate that, increasing the PVA content in the precursor (0 to 0.5 g) gave an obvious decrease of the band gap energy. Suddenly, the band gap energy increased with 1 g PVA. These changes in absorption edge may be associated with the corresponding changes in size of the synthesized materials [40,41]. Since decreased band gap energy corresponds to more redox ability for the production of photogenerated electron-hole pairs, reduced recombination effect and higher photoresponse [42], the 0.5PV/TiO_2 is expected to perform optimally.

Photocatalytic Kinetics

In order to ascertain the superior applicability of photocatalysis for the MO degradation, photolysis, and dark adsorption experiments were performed for 2 h and the results were compared. As shown in Fig. 10, there is no significant disappearance of methyl orange in the event of photolysis (< 4.8%) and adsorptive removal (3.4%). Conversely, there is a high decontamination in the photocatalytic regime based on the regular titania, 0PV/TiO_2 (86%), and in the PVA synthesized catalysts, 0.25PV/TiO_2 (89%) and 1PV/TiO_2 (91%). Ultimately, 0.5PV/TiO_2 derived using the optimal PVA offered the highest catalytic performance (97.2%). This may be attributed to its least band gap energy [40], as smaller particle size, high pore volume and surface area which will permit better absorption of dye molecules on the catalyst surface and penetration through the channels of the catalyst [4,19,43].

The kinetics of photocatalytic degradation of organic compounds usually follows the Langmuir-Hinshelwood scheme, which at low concentrations permits the application of the pseudo-first-order rate equation. However, conformity with pseudo-zero-order equation is kinetically possible at surface saturation. Following comparison of the coefficients of determination of various kinetic profiles, the degradation of MO in this study was found to agree with the zero-order kinetics (Fig. 11). Generally, the rate law for degradation of MO can be represented by Eq. (3) and the integrated zero-order rate law may take form Eq. (4).

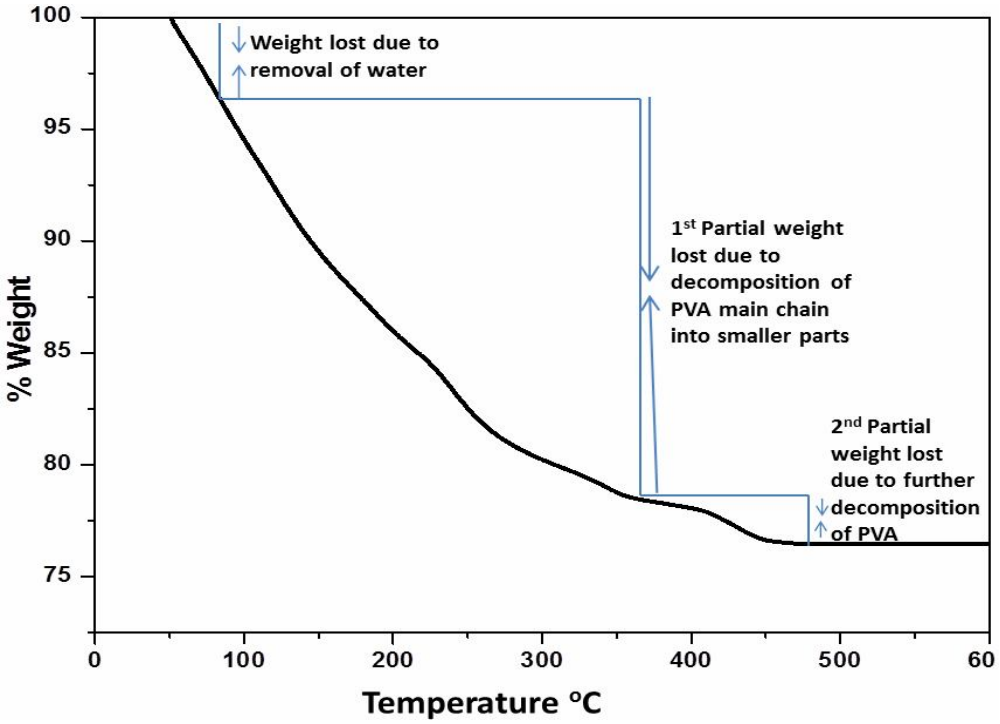

Fig. 8. Thermogram showing the effect of heat on the 0.5PV/TiO_2 precursor.

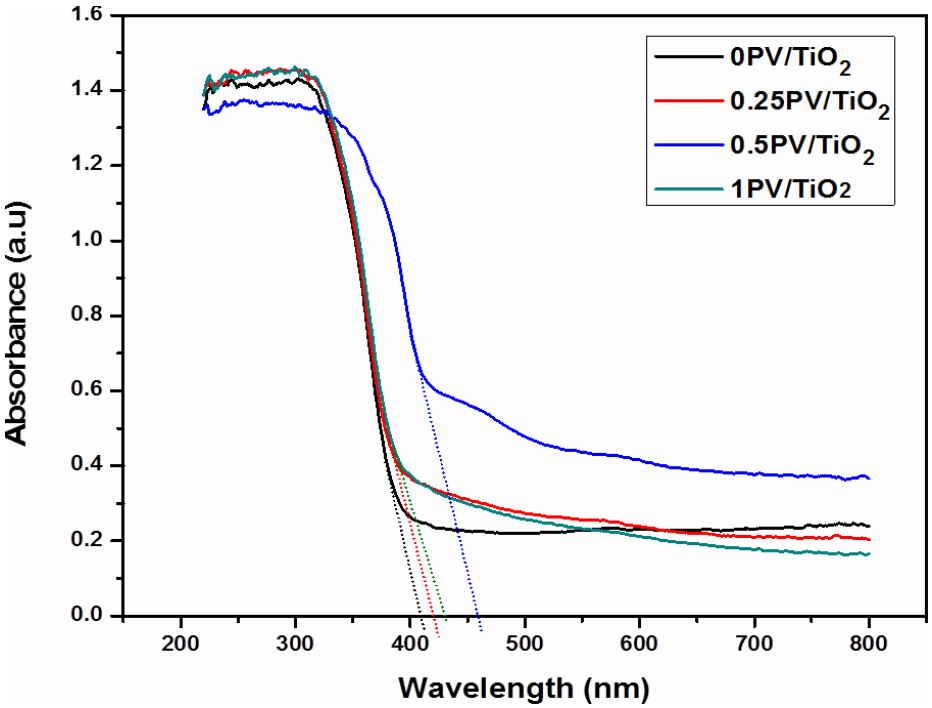

Fig. 9. UV-Vis spectra of the synthesized materials.

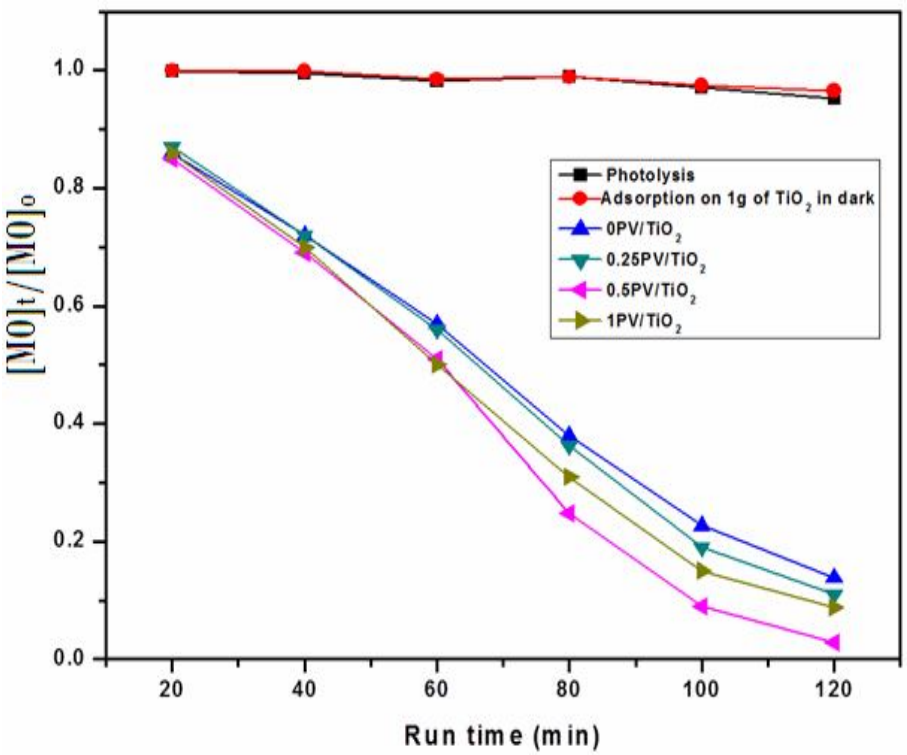

Fig. 10. Photocatalytic degradation of MO solution (25 mg l^{-1}) in the presence of the synthesized photocatalysts (1 g l^{-1}) at pH of 6.2 under 2 h UV exposure.

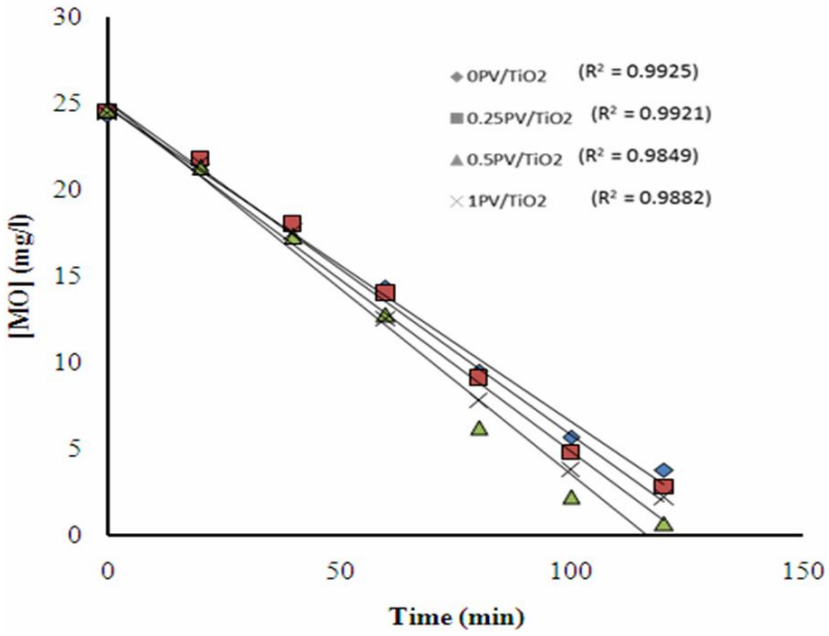

Fig. 11. Zero-order profiles of MO degradation in presence of different photocatalysts.

$$\frac{-d[MO]}{dt} = k \quad (3)$$

$$[MO]_t = -kt + [MO]_0 \quad (4)$$

where $[MO]_t$ and $[MO]_o$ are the concentrations (mg l^{-1}) at time t and when $t = 0$, respectively, and k is the zero-order constant (expressed as mg l^{-1} s^{-1}). A plot of [MO] *vs*. t gave a straight line with slope = $-k$ and intercept = $[MO]_o$ with R square values > 0.9 (Fig. 11), confirming the applicability of the zero-order kinetics to this study.

CONCLUSIONS

Highly photoactive ultrathin mesoporous titania with tunable band gap energy, particle size, pore volume, and surface area can be synthesized from $TiCl_3$ *via* precipitation and templating with poly(vinyl alcohol). This polymer has the capacity to direct the formation of controllable mesostructures and to restrict polymorph to the anatase form. The mesoporous structure of prepared titania is stable upon thermal detemplation. The particles of the prepared catalysts were plate-like discs confined to quantum dot vicinity.

ACKNOWLEDGMENTS

The authors acknowledge Universiti Putra Malaysia (UPM) where part of the work was conducted under the Mobility Program. Abubakar Hamisu gratefully acknowledges his sponsorship for PhD and benchwork by Kano State University of Technology through Nigerian Tertiary Education Trust Fund (TETFUND).

REFERENCES

[1] Pan, J. H.; Dou, H.; Xiong, Z.; Xu,; Ma, C. J.; Zhao, X., Porous photocatalysts for advanced water purifications. *J. Mater. Chem.* **2010**, *20*, 4512-4528. DOI: 10.1039/B925523K.

[2] Nguyen, D.; Wang, W.; Long, H.; Ru, H., Facile and controllable preparation of mesoporous TiO_2 using poly(ethylene glycol) as structure-directing agent and peroxotitanic acid as precursor. *Front. Mater. Sci.* **2016**, *10*, 405-412. DOI: 10.1007/s11706-016-0352-x.

[3] Tang, G.; Zhang, D.; Zhao, L.; Zhang, M.; Tang, H.; Huang, H.; Li, C., Template-free synthesis of uniform TiO_2 mesoporous microspheres with enhanced photocatalytic activity. *Mater. Lett.* **2014**, *118*, 192-195. DOI: 10.1016/j.matlet.2013.12.071.

[4] Chen, X.; Kuo, D. H.; Lu, D.; Hou, Y.; Kuo, Y. R., Synthesis and photocatalytic activity of mesoporous TiO_2 nanoparticle using biological renewable resource of un-modified lignin as a template. *Microporous Mesoporous Mater.* **2016**, *223* 145-151. DOI: 10.1016/j.micromeso.2015.11.005.

[5] Kumar, N.; Hazarika, S. N.; Limbu, S.; Boruah, R.; Deb, P.; Namsa, N. D.; Das, S. K., Hydrothermal synthesis of anatase titanium dioxide mesoporous microspheres and their antimicrobial activity. *Microporous Mesoporous Mater.* **2015**, *213*, 181-187. DOI: 10.1016/j.micromeso.2015.02.047.

[6] Feng, Z.; Wei, W.; Wang, L.; Hong, R., Hollow mesoporous titania microspheres: New technology and enhanced photocatalytic activity. *Appl. Surf. Sci.* **2015**, *357*, 759-765. DOI: 10.1016/ j.apsusc.2015.09.108.

[7] Antonelli, D. M.; Ying, J. Y., Synthesis of hexagonally packed mesoporous TiO_2 by a modified sol-gel method. *Angew. Chem., Int. Ed. Engl.* **1995**, *34*, 2014-2017. DOI: 10.1002/anie.199520141.

[8] Kumaresan, L.; Prabhu, A.; Palanichamy, M.; Murugesan, V., Synthesis of mesoporous TiO_2 in aqueous alcoholic medium and evaluation of its photocatalytic activity. *Mater. Chem. Phys.* **2011**, *126*, 445-452. DOI: 10.1002/anie.199520141.

[9] Zhang, K.; Wang, X.; Guo, X.; He, T.; Feng, Y., Preparation of highly visible light active Fe-N co-doped mesoporous TiO_2 photocatalyst by fast sol-gel method. *J. Nanopart. Res.* **2014**, *16*, 2246. DOI: 10.1007/s11051-014-2246-0.

[10] Wang, J.; Zhou, Y.; Hu, Y.; O'Hayre, R.; Shao, Z., Facile synthesis of nanocrystalline TiO_2 mesoporous microspheres for lithium-ion batteries. *J. Phys. Chem. C* **2011**, *115* 2529-2536. DOI: 10.1021/ jp1087509.

[11] Zi, S. C.; Chandren, S.; Yuan, L. S.; Razali, R.; Ho, C. S.; Hartanto, D.; Indra Mahlia, T. M.; Nur. H., New

method to synthesize mesoporous titania by photodegradation of surfactant template. *Solid State Sci.* **2016**, *52*, 83-91. DOI: 10.1016/ j.solidstatesciences.2015.12.016.

[12] Tian, C. X.; Yang, Y.; Pu, H., Effect of calcination temperature on porous titania prepared from industrial titanyl sulfate solution. *Appl. Surf. Sci.* **2011**, 257, 8391-8395.

[13] Masolo, E.; Senes, N.; Pellicer,E.; Baró, M. D.; Enzo, S.; Pilo, M. I.; Mulas, G.; Garroni, S., Evaluation of the anatase/rutile phase composition influence on the photocatalytic performances of mesoporous TiO_2 powders. *Int. J. Hydrogen Energy* **2015**, *40*, 14483-14491. DOI: 10.1016/j.matchemphys.2014.06.017

[14] Biswas, S.; Sundstrom, V.; De, S., Facile synthesis of luminescent TiO_2 nanorods using an anionic surfactant: Their photosensitization and photocatalytic efficiency. *Mater. Chem. Phys.* **2014**, *147*, 761-771. DOI: 10.1016/ j.matchemphys.2014.06.017.

[15] Preethi, T.; Abarna, B.; Rajarajeswari, G. R., Reprint of Influence of chitosan-PEG binary template on the crystallite characteristics of sol-gel synthesised mesoporous nanotitania photocatalyst. *Appl. Surf. Sci.* **2014**, *319*, 197-204. DOI: 10.1016/ j.apsusc.2014.07.190.

[16] Hamaloğlu, K. Ö.; Çelebi, B.; Sağ, E.; Tuncel, A., A new method for the synthesis of monodisperse-porous titania microbeads by using polymethacrylate microbeads as template. *Microporous Mesoporous Mater.* **2015**, *207*, 17-26. DOI: 10.1016/ j.micromeso.2015.01.001.

[17] Sifontes, A. B.; Rosales, M.; Mendez, F. J.; Oviedo, O.; Zoltan, T., Effect of calcination temperature on structural properties and photocatalytic activity of ceria nanoparticles synthesized employing chitosan as template. *J. Nanomater.* **2013**, *2013*, 1-9. DOI: 10.1155/2013/265797.

[18] Fujishima, A.; Zhang, X.; Tryk, D. A., TiO_2 photocatalysis and related surface phenomena. *Surf. Sci. Rep* **2008**, *63*, 515-582. DOI: 10.1016/ j.surfrep.2008.10.001.

[19] Feilizadeh, M.; Vossoughi, M.; Zakeri, S. M. E.; Rahimi, M., Enhancement of efficient Ag-S/TiO_2 nanophotocatalyst for photocatalytic degradation under visible light, *Ind. Eng. Chem. Res.* **2014**, *53*, 9578-9586. DOI: 10.1021/ie403720h.

[20] Gaya, U. I.; Abdullah A. H., Heterogeneous photocatalytic degradation of organic contaminants over titanium dioxide: a review of fundamentals, progress and problems. *J. Photochem. Photobiol., C* **2008**, *9*, 1-12. DOI: 10.1016/ j.jphotochemrev.2007.12.003.

[21] Hayashi, H.; Torii K., Hydrothermal synthesis of titania photocatalyst under subcritical and supercritical water conditions. *J. Mater. Chem.* **2002**, *12*, 3671-3676. DOI: 10.1039/B207052A.

[22] Xiao, J.; Peng, T.; R. Li, Peng, Z.; Yan, C., Preparation, phase transformation and photocatalytic activities of cerium-doped mesoporous titania nanoparticles. *J. Solid State Chem.* **2006**, *179*, 1161-1170. DOI: 10.1016/j.jssc.2006.01.008.

[23] Mao-Xiang, J.; Xue-Qin, J.; Wang-Xing, L.; Dong-Hong, L.; Zhou, W., Preparation and photocatalytic activity of mesoporous TiO_2 microspheres. *Micro Nanosyst.* **2009**, *1*, 12-16. DOI: 10.2174/ 1876402910901010012.

[24] Gautam, A.; Tripathy, P.; Ram, S., Microstructure, topology and X-ray diffraction in Ag-metal reinforced polymer of polyvinyl alcohol of thin laminates. *J. Mater. Sci.* **2006**, *41*, 3007-3016. DOI: 10.1007/ s10853-006-6768-4.

[25] Chang, S. H.; Tung, K. W.; Liao, B. S.; Chu, K. Y., Surface and protein adsorption properties of 316L stainless steel modified by polyvinyl alcohol and plasma-treated polyvinyl alcohol films, *Surf. Coat. Technol.* **2019**, *362*, 208-212. DOI: 10.1016/ j.surfcoat.2019.02.003.

[26] Chen, J.; Wang, J.; Li, Y.; Wang, X.; Zhuang, T.; Zhang, Q., W. Wang, Catalysis mechanism of oxidized polyvinyl alcohol by pseudomonas hydrolase: Insights from molecular dynamics and QM/MM analysis. *Chem. Phys. Lett.* **2019**, *721*, 49-56. DOI: 10.1016/j.cplett.2019.02.023.

[27] Schaper, C. D.; Miahnahri, A., Polyvinyl alcohol templates for low cost, high resolution, complex printing. *J. Vac. Sci. Technol., B: Microelectron. Nanometer Struct.-Process., Meas., Phenom.* **2004**, 3323-3326. DOI: 10.1116/1.1827218.

[28] Melezhyk, O. V.; Prudius, S. V.; Brei, V. V., Sol-gel polymer-template synthesis of mesoporous WO_3/ZrO_2. *Microporous Mesoporous Mater.* **2001**, *49*, 39-44. DOI: 10.1016/S1387-1811(01)00397-3.

[29] Pon-On, W.; Meejoo, S.; Tang, I. M., Formation of hydroxyapatite crystallites using organic template of polyvinyl alcohol (PVA) and sodium dodecyl sulfate (SDS). *Mater. Chem. Phys.* **2008**, *112*, 453-460. DOI: 10.1016/j.matchemphys.2008.05.082.

[30] Gaya, U. I.; Abdullah, A. H.; Zainal, Z.; Hussein, M. Z., Photocatalytic treatment of 4-chlorophenol in aqueous ZnO suspensions: Intermediates, influence of dosage and inorganic anions, *J. Hazard. Mater.* **2009**, *168*, 57-63. DOI: 10.1016/j.jhazmat.2009.01.130.

[31] Cano-Casanova, L.; Amorós-Pérez, A.; Ouzzine, M.; Lillo-Ródenas, M. A.; Román-Martínez, M. C., One step hydrothermal synthesis of TiO_2 with variable HCl concentration: Detailed characterization and photocatalytic activity in propene oxidation, *Appl. Catal. B: Environmental,* 2018, *220*, 645-653. DOI: 10.1149/2.0191802jes.

[32] Liu, L.; Zhang, Y.; Dong, S.; Zhang, B.; Meng, S.; Xu, J.; Gao, P.; Feng, Y., Template controlled synthesis of mesoporous TiO_2 particles for efficient photoanodes in dye sensitized solar cells. *J. Electrochem. Soc.* **2018**, *165*, F1-F6. DOI: 10.1149/2.0191802jes.

[33] Yu, J.; Zhang, L.; Cheng, B.; Su, Y., Hydrothermal preparation and photocatalytic activity of hierarchically sponge-like macro-/mesoporous titania. *J. Phys. Chem. C* **2007**, *111*, 10582-10589. DOI: 10.1021/jp0707889.

[34] Jaimy, K. B.; Ghosh, S.; Sankar, S.; Warrier, K., An aqueous sol-gel synthesis of chromium(III) doped mesoporous titanium dioxide for visible light photocatalysis. *Mater. Res. Bull.* **2011**, *46*, 914-921. DOI: 10.1016/j.materresbull.2011.02.030.

[35] Huang, T.; Mao, S.; Yu, J.; Wen, Z.; Lu, G.; Chen, J., Effects of N and F doping on structure and photocatalytic properties of anatase TiO_2 nanoparticles. *RSC Adv.* **2013**, *3* 16657-16664. DOI: 10.1039/C3RA42600A.

[36] Salman, S. A.; Bakr, N. A.; Abduallah, S. S., Study of thermal decomposition and FTIR for PVA-AlCl composite films. *J. Eng. Appl. Sci.* **2019**, *14*, 717-724. DOI: 10.3923/jeasci.2019.717.724.

[37] Cui, S.; Wei, P.; Li, L., Thermal decomposition behavior of poly(propylene carbonate) in poly(propylene carbonate)/poly(vinyl alcohol) blend. *J. Therm. Anal. Calorim.* **2019**, *135*, 2437-2446. DOI: 10.1007/s10973-018-7297-5.

[38] Fernandes, D.; Hechenleitner, A. W.; Pineda, E. G., Kinetic study of the thermal decomposition of poly (vinyl alcohol)/kraft lignin derivative blends. *Thermochim. Acta* **2006**, *441*, 101-109. DOI: doi.org/10.1016/j.tca.2005.11.006.

[39] Feilizadeh, M.; Vossoughi, M.; Zakeri, S. M. E.; Rahimi, M., Enhancement of efficient Ag-S/TiO_2 nanophotocatalyst for photocatalytic degradation under visible light. *Ind. Eng. Chem. Res.* **2014**, *53*, 9578-9586. DOI: 10.1021/ie403720h.

[40] Bakre, P. V.; Tilve, S., Direct access to highly crystalline mesoporous nano TiO_2 using sterically bulky organic acid templates. *J. Phys. Chem. Solids* **2018**, *116*, 234-240. DOI: doi.org/10.1016/j.jpcs.2018.01.043.

[41] Thamaphat, K.; Limsuwan, P.; Ngotawornchai, B., Phase characterization of TiO_2 powder by XRD and TEM. *Kasetsart J. (Nat. Sci.)* **2008**, *42*, 357-361. DOI: kasetsartjournal.ku.ac.th/kuj_files/2009/A0903200935177812.

[42] Zhao, X.; Wu, P.; Liu, M.; Lu, D.; Ming, J.; Li, C.; Ding, J.; Yan, Q.; Fang, P., Y_2O_3 modified TiO_2 nanosheets enhanced the photocatalytic removal of 4-chlorophenol and Cr(VI) in sun light. *Appl. Surf. Sci.* **2017**, *410*, 134-144. DOI: 10.1016/j.apsusc.2017.03.073.

[43] Gao, M.; Zhu, L.; Ong, W. L.; Wang, J.; Ho, G. W., Structural design of TiO_2-based photocatalyst for H_2 production and degradation applications. *Catal. Sci. Technol.* **2015**, *5*, 4703-4726.